Communication

Al/C60 Nanocomposites Fabricated by High-Pressure Torsion

HAMED ASGHARZADEH, SOO-HYUN JOO, and HYOUNG SEOP KIM

Al-2 vol pct fullerene (C60) composites with relative densities of >0.98 are manufactured by high-pressure torsion of ball-milled powders under an applied pressure of 6 GPa. A considerable Al grain refinement to ~53 nm and a homogeneous distribution of fullerenes give rise to a very high hardness of 152 Hv and yield stress of 405 MPa. Nevertheless, the poor tensile ductility due to the low work-hardening rate is achieved.

DOI: 10.1007/s11661-015-2804-9

Fullerenes in the buckyball structure are composed of atomic arrangement of carbon into pentagons and hexagons in the form of a hollow sphere. Since the discovery of fullerenes in 1985 by Kroto *et al.*,[1] a considerable attention has been focused on their synthesis, characterization, and applications. A significant potential application of fullerenes is as reinforcement in metallic alloys for structural parts.[2] The production of metal matrix composites (MMCs) reinforced with fullerenes has been a subject of numerous investigations in the recent years.[2–5] Several methods have been used for the fabrication of these composites including codeposition,[3] squeeze casting,[4] and powder metallurgy.[5] In these techniques, the materials are exposed to high temperatures for relatively long periods, which cause a deleterious chemical reaction between fullerenes and metal matrix due to high reactivity and large surface area of fullerenes. For instance, formation of Al_4C_3 carbides has been reported during preparation of Al/C60 composites,[4] which may act as the preferred regions for initiation and propagation of microcracks. Furthermore, the fullerene molecules are unstable in the matrix during processing at high temperatures.[6]

An alternative route for manufacturing of fullerene-reinforced MMCs at low temperatures is severe plastic deformation (SPD). Utilizing of SPD techniques not only hinders the formation of detrimental phases, but also uniformly disperses the fullerene within the matrix and significantly refines the matrix microstructure. Morisada *et al.*[7] have dispersed fullerene into Al5083 by friction stir processing (FSP) and have shown a remarkable increase of hardness by both the grain refinement and the dispersion of fullerene molecules. Tokunaga *et al.*[8] have used high-pressure torsion (HPT) for consolidation of Al-fullerene powders. Although a significant Al grain refinement took place, they have stated the inhomogeneous distribution of fullerenes within the matrix.

The aim of this study is to fabricate fullerene-reinforced MMCs with a homogeneous distribution of reinforcement molecules within the Al matrix using HPT. In this method, intense shear strains are imposed to a sample located between two anvils rotating under a high pressure. For improvement of fullerenes' dispersion, high-energy ball milling (HEBM) of Al and fullerene powder mixtures was performed prior to HPT. HEBM has a great potential for dispersing various reinforcements into the matrix by repeated cycles of welding-fracture-rewelding of the particles.[9] The microstructural features and mechanical properties of the Al-fullerene nanocomposites were investigated.

The aluminum (>99 pct) and fullerene (99.9 pct) powders were used as starting materials. Fullerenes were dispersed in ethanol by using an ultrasonic shaker for 1 hour, and then Al powders were added into the dispersion and sonicated for 0.5 hour. After drying, Al-2 vol pct, fullerene powder mixtures with 10-mm-diameter steel balls were placed in milling vials in order to give a ball-to-powder weight ratio of 10:1. One weight percent stearic acid was added to prevent powder sticking to the balls and the vial walls. The vials were filled with argon and were agitated using a planetary ball mill at 350 rpm for 4 hours. The powders were degassed at 723 K (450 °C) for 1 hour and were stored in an argon-filled glove box.

The HPT consolidation was conducted under a quasi-constrained condition where there was some limited outward flow between the upper and lower anvils. 0.3 g of the Al-fullerene powder mixture was precompacted into disk-shaped samples 10 mm in diameter and 1.5 mm in thickness and then was placed between HPT anvils with a circular shallow hole, 10 mm in diameter and 0.25 mm deep. The compression was performed under an applied pressure of 6 GPa at room temperature. Simultaneously, the lower anvil was rotated with a rotational speed of 1 rpm by 1 to 15 turns, and surface friction forces deformed the disk by shear under quasi-hydrostatic pressure. Consolidation of HEBMed powders by HPT produced thin disk samples 10 mm in diameter and ~0.8 mm in thickness.

The density of disks was measured using a Mettler Toledo XP205 density meter. The microhardness was measured across the diameter of each disk with an applied load of 2.94 N using a Vickers indenter (Future-Tech FM-700, Japan). The tensile test was conducted using an Instron (8862 High-Precision Electric Actuator Systems, MA) machine operated at an initial strain rate of 10^{-3} s^{-1}. Four microtensile samples of a dog-bone shape with a 1.5-mm gage length and 1-mm width were

HAMED ASGHARZADEH, Assistant Professor, is with the Department of Materials Engineering, University of Tabriz, Tabriz 51666-16471, Iran. Contact e-mail: asgharzadeh@tabrizu.ac.ir SOO-HYUN JOO, Postdoc Researcher, and HYOUNG SEOP KIM, Professor, are with the Department of Materials Science and Engineering, Pohang University of Science and Technology (POSTECH), Pohang 790-784, South Korea. Contact e-mail: hskim@postech.ac.kr

Manuscript submitted November 9, 2014.
Article published online February 18, 2015

cut from the disks using electro discharge machining (EDM) at a distance of 2.5 mm from the center. The samples were polished for removing surface defects that may be introduced by EDM to a 0.5-mm thickness. During the tensile test, precise strains were measured by ARAMIS 5 M (GOM mbH, Germany) vision strain system using the digital image correlation (DIC) method. Before testing, a random black-and-white speckled pattern was created on the surface of the tensile samples in order to accurately measure local coordinates in the DIC method. The fracture surface of the tensile samples was examined using a field emission scanning electron microscope (FE-SEM, JEOL JSM-6330F, Japan).

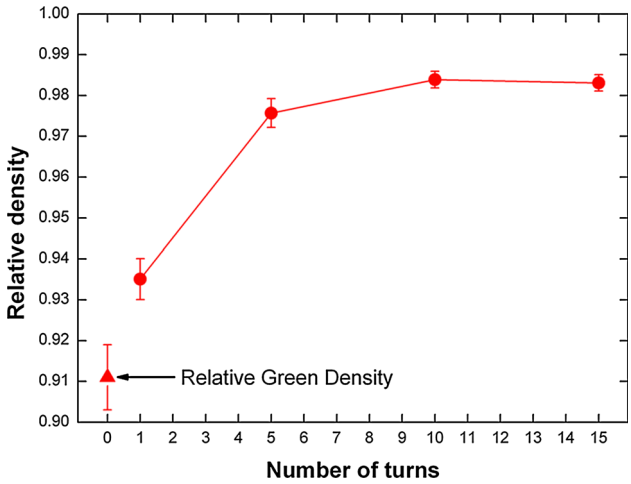

Fig. 1—Relative density of Al-Fullerene as a function of number of turns.

The polished samples were etched using a solution of 1 pct HF in distilled water, and the microstructure was observed using optical microscope (OM, Olympus BX61, Japan). The internal microstructures of the disks were examined by scanning transmission electron microscopy (STEM, JEOL JEM 2100F TEM, Japan) operating at 200 kV. The STEM specimens were prepared by dual beam focused ion beam milling, using a 3D Total Analysis (Helios Nanolab Dual Beam, FEI, Hillsboro, OR) cut from the HPT disks at a distance of 2.5 mm from the center.

Figure 1 shows the variation of relative density (RD) of Al-fullerene against the number of turns (N). The RD of compacts increased from 0.911 to 0.935 after HPT for $N = 1$. While a significant densification was attained after $N = 5$, consecutive straining to 15 turns slightly increased the density of HPT disks. Near-full density disks with a RD of 0.984 were achieved due to the severe straining, concurrent with the large pressure imposed by the HPT process. Moreover, the scatter of the RD decreased with the increasing N.

The Al-fullerene powders present flattened morphology with an average particle size of ~100 μm (Figure 2(a)), revealing predomination of plastic deformation mechanism upon HEBM. After HPT consolida-

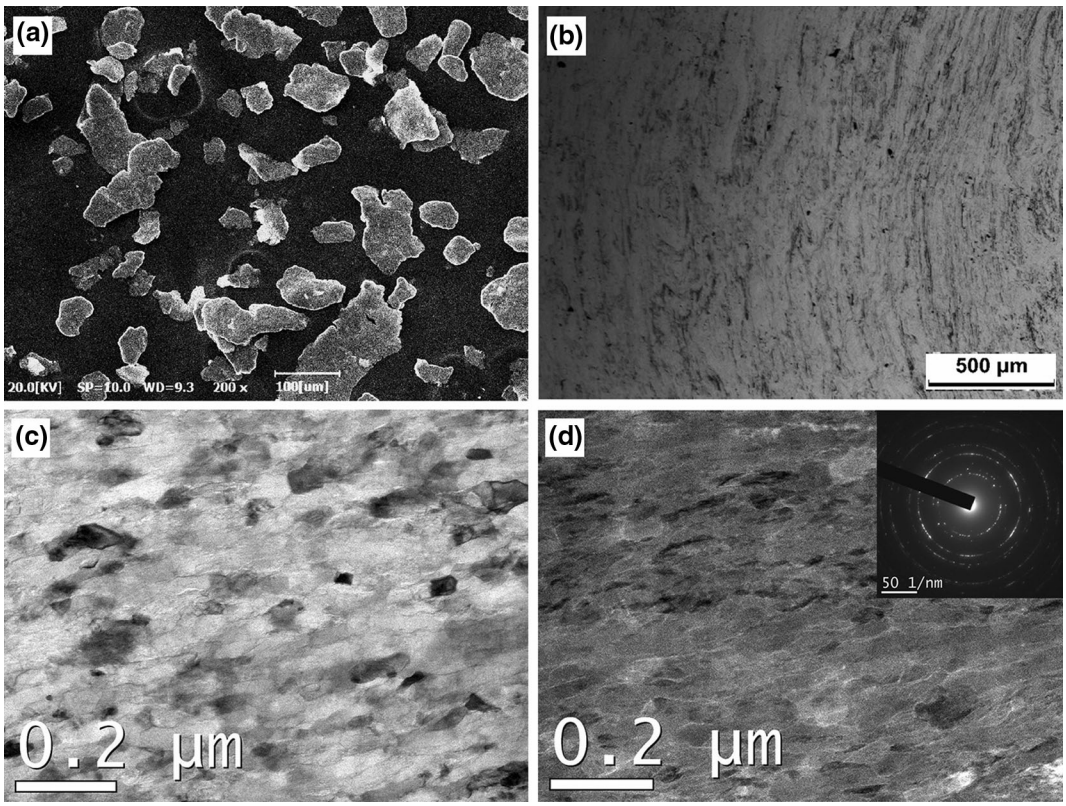

Fig. 2—(*a*) SEM micrograph from Al-Fullerene powder; (*b* through *d*) microstructure of HPT Al-Fullerene disk processed for 10 turns in the middle region: (b) OM image; (c) BF-STEM image; and (d) HAADF image including SAD pattern.

tion for 10 turns, the powders were well bonded together, and the prior particle boundaries were not visible (Figure 2(b)) due to the severe shear straining upon HPT. Representative brightfield (BF) and high-angle-angular-dark-field (HAADF) TEM micrographs after HPT for 10 turns (Figures 2(c) and (d)) illustrate that HPT deformation gives rise to a significant grain refinement. Although some of very fine grains (<~50 nm) are equiaxed, most of the grains are flattened in a direction perpendicular to the compression axis. The size range of the grains is from 10 to 350 nm, more frequently, from 10 to 50 nm. The average length and thickness of grains were measured from 100 grains, and determined to be 86 ± 60 nm and 33 ± 17 nm, respectively. The wide grain size distribution can be because all the grains have different orientations and receive locally different loading conditions, although the overall external loading is homogeneous. This grain size is smaller than the grain sizes in pure Al (~287 nm) and Al-3 vol pct carbon nanotube (~65 nm) processed similarly.[10] The grain structure is also finer than Al-5 wt pct fullerene processed by HPT under an applied pressure of 2.5 GPa for 15 turns (~80 nm[8]) and Al5083-fullerene fabricated by FSP under the travel speed of 50 mm min^{-1} and the tool rotating rate of 1500 rpm (~200 nm[7]). The SAD pattern, shown as inset in Figure 2(d), exhibits continuous rings from individual spots due to the FCC Al phase indicator of grains separated by high-angle grain boundaries.

The Vickers microhardness, Hv, values are shown in Figure 3(a) where the lower line shows the initial microhardness for the Al-fullerene powder before HPT. These plots exhibit that the Hv increases from the center to the edge of the disk. Moreover, microhardness significantly increases with N, especially in the central regions. It is apparent that the error bars are larger in the central regions, and decrease with an increase in N, revealing a gradual transition to microstructural uniformity after large numbers of turns. For the 10- and 15-turn disks and beyond a distance of 4 mm from the center, the Hv values appear to reach saturation at Hv $\approx$ 152. This hardness is larger than the maximal hardness values of fullerene-reinforced pure Al (118 Hv[8]) and Al5083 (135 Hv[7]) matrix composites processed by HPT and FSP, respectively. In processing by HPT, the shear strain imposed on a disk, γ, is estimated by $\gamma = 2\pi Nr/h$,[11] where r is the distance from the center of the disk, and h is the thickness of the disk. By considering an average value of $h \approx 0.8$ mm, the equivalent von Mises strain, $\varepsilon_{eq} = \gamma/\sqrt{3}$, was calculated, and the Hv values were re-plotted against ε_{eq} (Figure 3(b)). It is clear that a significant strain hardening occurs at the lower ε_{eq} and then reaches a constant value of ~152 Hv at $\varepsilon_{eq} > \sim 100$. This behavior is typical of a very wide range of metals and MMCs where recovery processes cannot easily occur.[12]

Figure 4(a) shows tensile stress–strain curve of Al-2 vol pct fullerene composite at room temperature. A rapid hardening occurred during deformation, and a very high tensile strength of 409 MPa was achieved. Interestingly, this strength is approximately 63 pct higher than that of Al-5 wt pct fullerene processed

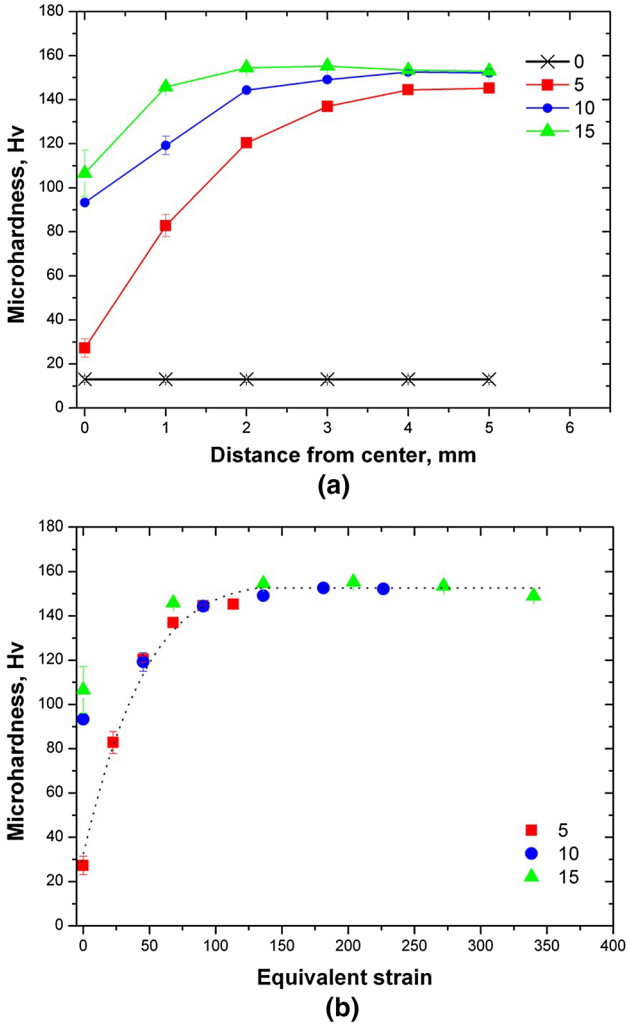

Fig. 3—Variation of Vickers microhardness with (*a*) distance from the center of the disks; and (*b*) the equivalent von Mises strain after the HPT process for various numbers of turns.

through HPT.[8] It has been proposed to estimate the yield stress, σ_y, as the sum of contributions from multiple strengthening mechanisms, including grain boundary strengthening (σ_b), dislocation strengthening (σ_ρ), and dispersion hardening (σ_d) expressed in the equations[13,14]:

$$\sigma_y = \sigma_0 + \sigma_b + \sigma_\rho + \sigma_d = \sigma_0 + k_y d^{-1/2} + \alpha G b \rho^{1/2} + \frac{0.158\, Gm\, b \ln\left(\frac{\phi}{2b}\right)}{\phi(f^{-1/2} - 1)}, \quad [1]$$

where σ_0 is the friction stress (20 MPa[15]), k_y is the Hall–Petch coefficient (0.04 MPa$\sqrt{\text{m}}$[15]), d is the grain size, α is a constant (0.93[16]), G is the shear modulus (25.8 GPa), b is the Burgers vector (0.286 nm), ρ is the dislocations' density (estimated by the line intercept method,[17] $\approx 5 \times 10^{14}$ m^{-2}), m is the Taylor factor (3.06[12]), Φ is the diameter of fullerene (8 to 15 nm), and f is the concentration of fullerene (0.02). In this analysis, the role of dispersion of thin oxide layer initially

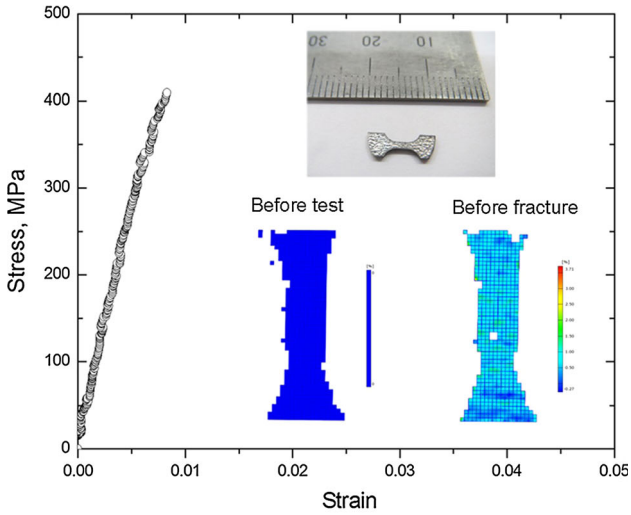

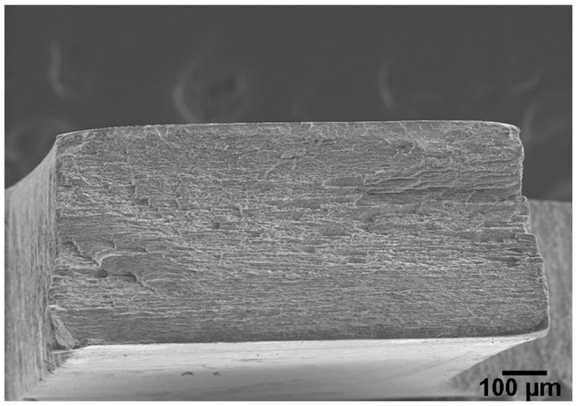

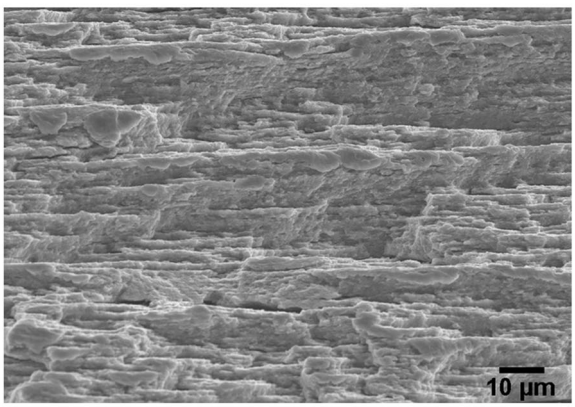

Fig. 4—(*a*) Engineering tensile stress–strain curve of Al-fullerene nanocomposite processed by HPT for 10 turns with a tensile test specimen and Mises equivalent strain distributions before the test and before the fracture as insets; (*b*) fracture surface after tensile testing; and (*c*) fracture surface at higher magnification.

present on the surface of gas-atomized Al powders has not been considered. The yield stress of Al-2 vol pct fullerene has been calculated to be 430 MPa, which is in convincing agreement with an experimental value, 405 MPa. It should be stated that the grain boundary strengthening and hardening resulting from fullerene particles are the dominant strengthening mechanisms with a relatively similar contribution (~40 pct).

Inspection of the stress–strain curve indicates that a slight strain hardening takes place in contrast to the pure Al sample that exhibited an extensive strain-hardening behavior described elsewhere.[10] The time of absorption of dislocations by grain boundaries during tensile deformation can be expressed as $t = \rho bd/c\dot{\varepsilon}$,[18] where c is a geometric factor, and $\dot{\varepsilon}$ is the strain rate. Taking $c = 2.4$ and $\dot{\varepsilon} = 10^{-3}\ s^{-1}$, t was estimated to be less than 1 second which is much smaller than the tensile deformation time (~135 second). Accordingly, the dislocations trapped at grain boundaries would have enough time to spread into the grain boundaries during tensile deformation, resulting in a limited dislocation accumulation and strain hardening.

The equivalent strain distribution on the surface of the tensile specimen obtained from the DIC analysis (indicated as inset in Figure 4(a)) revealed that only a slight plastic deformation was accumulated in the specimen so that little-to-no necking took place. Thus, the smooth fracture surface with a fracture path perpendicular to the loading direction was accomplished (Figure 4(b)). Although some shallow and fine dimples were observed on the SEM fractographs at a higher magnification (Figure 4(c)), the fracture surface predominantly appeared to be cleaved. The poor tensile ductility at room temperature has been reported previously in several nanocrystalline materials,[19,20] being attributed to the processing artifacts, tensile instability, and crack shear instability.[21] Here, the low work-hardening rate as a consequence of a little interaction of dislocations within the grain interior after plastic deformation is principally responsible for the poor ductility of Al-fullerene composite.

In summary, the microstructure and mechanical properties of Al-2 vol pct fullerene composite fabricated by HPT were investigated. A high degree of densification and a substantial grain refinement were obtained after the HPT process for 10 turns under the applied pressure of 6 GPa. Evaluating the mechanical properties indicated an improvement of ~93 pct in the yield stress and 58 pct in the hardness of the Al-fullerene composites over the unreinforced Al, which was mainly attributed to the grain boundary and Orowan strengthening mechanisms.

This study was supported by the National Research Foundation of Korea (NRF) grant funded by the Korea government (MSIP) (No. 2014R1A2A1A10051322). H.A. thanks the University of Tabriz (Iran) for all of the support provided.

REFERENCES

1. H.W. Kroto, J.R. Heath, S.C. O'Brien, R.F. Curl, and R.E. Smalley: *Nature*, 1985, vol. 318, pp. 162–63.

2. E.V. Barrera, J. Sims, and D.L. Callahan: *J. Mater. Res.*, 1995, vol. l0, pp. 366–71.
3. J.G. Hou, X. Li, H. Wang, and B. Wang: *J. Phys. Chem. Solids*, 2000, vol. 61, pp. 995–98.
4. F.A. Khalid, O. Beffort, U.E. Klotz, B.A. Keller, P. Gasser, and S. Vaucher: *Acta Mater.*, 2003, vol. 51, pp. 4575–82.
5. H. Watanabe, M. Fukusumi, K. Ishikawa, and T. Shimizu: *Scripta Mater.*, 2006, vol. 54, pp. 1575–80.
6. K. Miyazawa, J. Yano, I. Honma, and M. Akaishi: *J. Am. Ceram. Soc.*, 2000, vol. 83, pp. 2315–17.
7. Y. Morisada, H. Fujii, T. Nagaoka, K. Nogi, and M. Fukusumi: *Composites A*, 2007, vol. 38, pp. 2097–101.
8. T. Tokunaga, K. Kaneko, K. Sato, and Z. Horita: *Scripta Mater.*, 2008, vol. 58, pp. 735–38.
9. C. Suryanarayana: *Prog. Mater Sci.*, 2001, vol. 46, pp. 1–184.
10. H. Asgharzadeh, S.H. Joo, and H.S. Kim: *Metall. Mater. Trans. A*, 2014, vol. 45A, pp. 4129–37.
11. R.Z. Valiev, Y.V. Ivanisenko, E.F. Rauch, and B. Baudelet: *Acta Mater.*, 1996, vol. 44, pp. 4705–12.
12. M. Kawasaki, J. Foissey, and T.G. Langdon: *Mater. Sci. Eng. A*, 2013, vol. 561, pp. 118–25.
13. H. Asgharzadeh, A. Simchi, and H.S. Kim: *Mater. Charact.*, 2013, vol. 75, pp. 108–14.
14. I. Gutierrez-Urrutia, M.A. Muñoz-Morris, and D.G. Morris: *J. Mater. Res.*, 2006, vol. 21, pp. 329–42.
15. N.J. Petch: *J. Iron Steel Inst.*, 1953, vol. 174, pp. 25–28.
16. Y. Li, Y.H. Zhao, V. Ortalan, W. Liu, Z.H. Zhang, R.G. Vogt, N.D. Browning, E.J. Lavernia, and J.M. Schoenung: *Mater. Sci. Eng. A*, 2009, vol. 527, pp. 305–16.
17. B.P. Kashyap, P.D. Hodgson, Y. Estrin, I. Timokhina, M.R. Barnett, and I. Sabirov: *Metall. Mater. Trans. A*, 2009, vol. 40A, pp. 3294–303.
18. R.Z. Valiev, R.K. Islamgaliev, and I.V. Alexandrov: *Prog. Mater Sci.*, 2000, vol. 45, pp. 103–89.
19. M.A. Meyers, A. Mishra, and D.J. Benson: *Prog. Mater Sci.*, 2006, vol. 51, pp. 427–556.
20. C.Y. Yu, P.W. Kao, and C.P. Chang: *Acta Mater.*, 2005, vol. 53, pp. 4019–28.
21. C.C. Koch: *Nanocryst. Mater.*, 2003, vol. 18, pp. 9–20.